

A Cu₃BHT-Graphene van der Waals Heterostructure with Strong Interlayer Coupling

Zhiyong Wang^{1,2}, Shuai Fu^{2,3}, Wenjie Zhang¹, Baokun Liang⁴, Tsai-Jung Liu², Mike Hambsch⁵, Jonas F. Pöhls⁶, Yufeng Wu¹, Jianjun Zhang², Tianshu Lan¹, Xiaodong Li^{1,2}, Haoyuan Qi⁴, Miroslav Polozij^{2,9}, Stefan C. B. Mannsfeld⁵, Ute Kaiser⁴, Mischa Bonn³, R. Thomas Weitz⁶, Thomas Heine^{2,9,10}, Stuart S. P. Parkin^{1*}, Hai I. Wang^{3,7*}, Renhao Dong^{2,8*}, Xinliang Feng^{1,2*}

¹Max Planck Institute for Microstructure Physics, Halle (Saale), Germany.

²Center for Advancing Electronics Dresden (cfaed) and Faculty of Chemistry and Food Chemistry, Technische Universität Dresden, Dresden, Germany.

³Max Planck Institute for Polymer Research, Mainz, Germany.

⁴Central Facility for Electron Microscopy, Electron Microscopy of Materials Science, Ulm University, Ulm, Germany.

⁵Center for Advancing Electronics Dresden, Technische Universität Dresden, Dresden, Germany.

⁶First Institute of Physics, Georg August University of Göttingen, Göttingen, Germany.

⁷Nanophotonics, Debye Institute for Nanomaterials Science, Utrecht University, Utrecht, the Netherlands.

⁸Key Laboratory of Colloid and Interface Chemistry of the Ministry of Education, School of Chemistry and Chemical Engineering, Shandong University, Jinan, China.

⁹Helmholtz-Zentrum Dresden-Rossendorf, Institute of Resource Ecology, Leipzig, Germany.

¹⁰Department of Chemistry, Yonsei University, Seoul, Republic of Korea.

*E-mail: stuart.parkin@mpi-halle.mpg.de; h.wang05@uu.nl; renhaodong@sdu.edu.cn; xinliang.feng@tu-dresden.de

Two-dimensional van der Waals heterostructures (2D vdWhs) are of significant interest due to their intriguing physical properties that are critically defined by the constituent monolayers and their interlayer coupling. However, typical inorganic 2D vdWhs fall into the weakly coupled region, limiting efficient interfacial charge flow—crucial for developing high-performance quantum optoelectronics. Here, we demonstrate strong interlayer coupling in Cu₃BHT (BHT = benzenehexathiol)-graphene vdWhs, an organic-inorganic bilayer characterized by prominent interlayer charge transfer. Monolayer Cu₃BHT with a Kagome lattice is synthesized on the water surface and then coupled with graphene to produce a cm²-scale 2D vdWh. Spectroscopic and electrical studies, along with theoretical calculations, show significant hole transfer from monolayer Cu₃BHT to graphene upon contact, being characteristic fingerprints for strong interlayer coupling. This study unveils the great potential of integrating highly π -conjugated 2D coordination polymers (2DCPs) into 2D vdWhs to explore intriguing physical phenomena.

Two-dimensional van der Waals heterostructures (2D vdWhs) constitute a new class of artificial materials constructed by vertically stacking atomically thin 2D crystals, including graphene, transition metal dichalcogenides (TMDs), and hexagonal boron nitride (*h*-BN) which are held together by vdW interactions^{1,2}. The lack of direct chemical bonding in vdWhs affords complete freedom in the selection of 2D materials, unrestricted by constraints of crystal symmetry, structure, and lattice matching³. Thanks to their atomically thin nature, the properties of vdWhs can be tailored by not only individual constituents but also interlayer coupling, giving

rise to new quantum states and phenomena⁴. These unique characteristics have established vdWhs as a versatile platform for a wide spectrum of applications, including tunneling transistors⁵, photodetectors,⁶ and light-emitting devices⁷ with unprecedented functionalities. While vdWhs hold great promise for developing new materials and device concepts, the fabrication of high-quality monolayer 2D crystals is limited by the exfoliation of existing bulk-layered crystals, which restricts the scope and progress of vdWhs research. In addition, further exploration of 2D vdWhs is still impeded by the usually weak interlayer coupling and the lack of control in tuning the interlayer interactions⁸⁻¹⁰. Hence, the discovery of novel vdWhs that enable manipulation of band alignment and interlayer electronic coupling is a topic of great research interest.

Here, we exploit the synergistic effect of highly delocalized electronic orbitals in Cu₃BHT and massless Dirac Fermions in graphene to target strongly coupled organic-inorganic bilayers. We show that vertically stacking monolayer Cu₃BHT and graphene through a wet transfer technique enables the creation of cm²-scale Cu₃BHT-graphene vdWhs with intimate and uniform contacts. Raman and terahertz time-domain spectroscopy (THz-TDS) studies, combined with electrical measurements and theoretical modeling, demonstrate significant hole transfer from monolayer Cu₃BHT to graphene upon contact, leading to a downshift of the Fermi level (E_F) in graphene arising from the strong interlayer electronic coupling. These findings open up new possibilities for exploring novel 2D vdWhs with manipulable orbital distribution, interfacial band alignment, and interlayer coupling, a cornerstone for developing and envisioning novel quantum optoelectronics.

Results and discussion

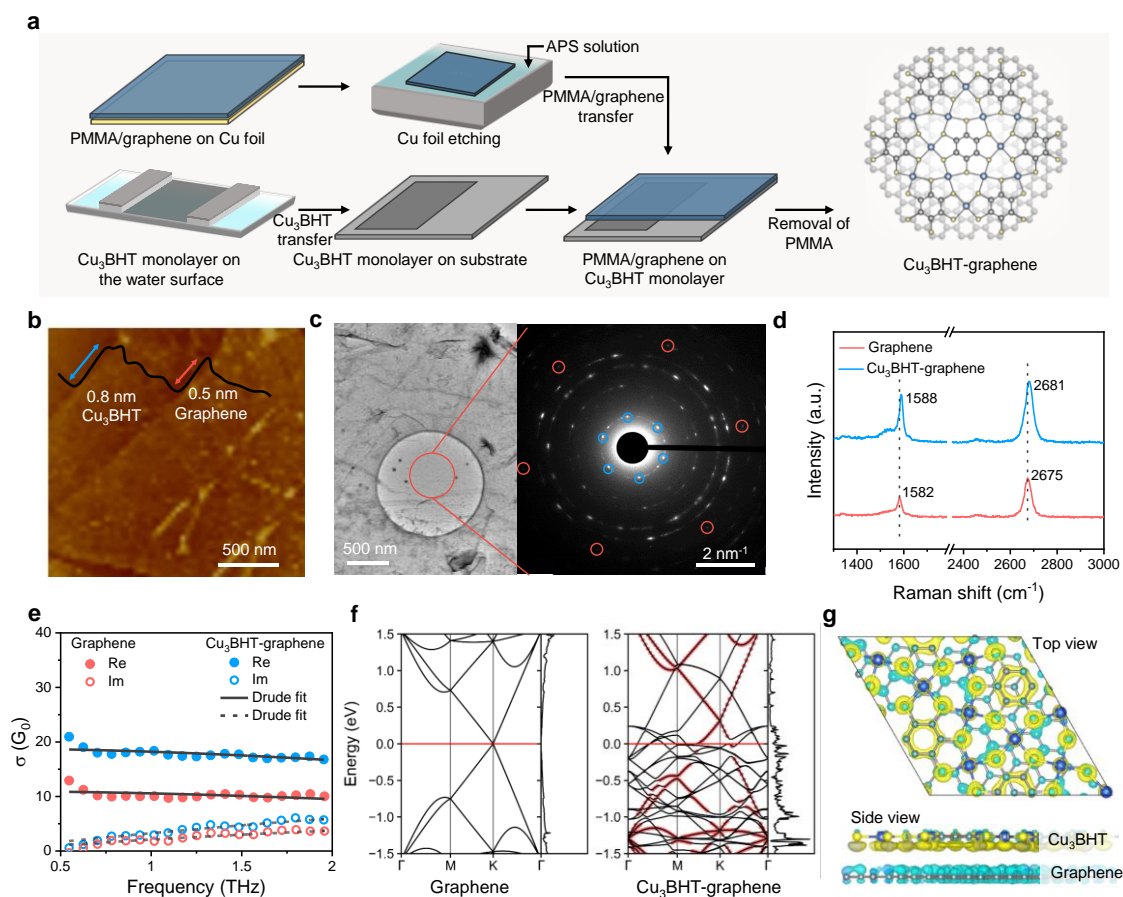


Figure 1| Morphological and interlayer coupling characterization of Cu₃BHT-graphene

vdWh. a, Schematic of the preparation of Cu₃BHT-graphene vdWh by a wet transfer technique. **b**, AFM image and height profile of monolayer Cu₃BHT (blue line) and graphene (yellow line) in the vdWh. **c**, TEM image and corresponding SAED pattern of Cu₃BHT-graphene vdWh. **d**, Raman spectra of graphene before and after deposition of monolayer Cu₃BHT. In the vdWh, the well-preserved symmetry of the G- and 2D-modes indicates that graphene maintains its structural integrity after contact with Cu₃BHT. **e**, Frequency-resolved complex sheet conductivity $\sigma_s(w)$ of bare graphene (red) and Cu₃BHT-graphene vdWh (blue) in units of quantum conductance $G_0 = 2e^2/h$. The solid and dashed lines correspond to the Drude fits of the real and imaginary parts of $\sigma_s(w)$, respectively. **f**, Band structures of graphene and graphene-Cu₃BHT vdWh with 3° twist angle and their corresponding densities of states (DOS). Red dots in graphene-Cu₃BHT vdWh band structure indicate bands originating predominantly from the graphene layer. **g**, The CDD of Cu₃BHT-graphene vdWh. Charge density isosurfaces value is set to 0.0003 e Bohr⁻³ with yellow and blue showing increase and decrease of electron density, respectively.

We fabricated the vdWh by combining monolayer Cu₃BHT synthesized on the water surface with large-area chemical vapor deposited (CVD) graphene using a wet transfer technique (Fig. 1a). The resulting vdWh was then washed and annealed at 300 °C under H₂-Ar atmosphere to remove PMMA and trapped interfacial contaminants, and to enhance the interaction between Cu₃BHT and graphene. Fig. 1b shows the morphology of Cu₃BHT-graphene vdWh, from which the monolayer nature of both Cu₃BHT and graphene layers was confirmed. We further characterized the structures of Cu₃BHT-graphene vdWh using SAED and TEM (Fig. 1c, left). The SAED pattern from the overlapping Cu₃BHT-graphene region shows two sets of diffraction spots (Fig. 1c, right), with the inner and outer sets corresponding to Cu₃BHT and graphene, respectively. Note that no clear Moiré superlattice structure was observed using AC-HRTEM imaging, mainly due to the limited domain size (tens of nm) of the polycrystalline Cu₃BHT¹¹⁻¹⁴.

We conducted Raman and THz measurements to study the electron re-equilibrium upon vdWh formation. Raman spectra of graphene, taken before and after deposition of monolayer Cu₃BHT, were averaged from Raman mapping images and presented in Fig. 1d. Pristine graphene exhibits G- and 2D-modes at 1,582 cm⁻¹ and ~2,675 cm⁻¹, respectively, indicative of high-quality monolayer graphene with negligible strain and doping effects^{15,16}. The deposition of monolayer Cu₃BHT resulted in a blue-shift (~6 cm⁻¹) of both G- (~1,588 cm⁻¹) and 2D (2,681 cm⁻¹)-modes, indicating an increased hole concentration in graphene¹⁵. By deconvoluting the contributions of strain and doping using the correlation between G-mode and 2D-mode¹⁶, we find that monolayer Cu₃BHT coverage on graphene introduces negligible strain but substantial hole density modulation, whereby the E_F in graphene shifts downward by ~0.29 eV in vdWh (equivalent to a hole concentration of ~5 × 10¹² cm⁻²).

To gain deeper insight into the ground-state charge transfer (CT) effect upon vdWh formation, we employ time-resolved THz spectroscopy (TRTS) to investigate the frequency-resolved complex sheet conductivity $\sigma(\omega)$ of graphene with and without monolayer Cu₃BHT interactions. Given the negligible intrinsic conductivity of monolayer Cu₃BHT, the observed THz absorption (and thus conductivity) in bare graphene and Cu₃BHT-graphene vdWh can be attributed to the presence of conductive charge carriers in the graphene layer. As shown in Fig. 1e, $\sigma(\omega)$ of bare graphene and Cu₃BHT-graphene vdWh can be well described by the Drude model (equation 1)^{17,18}.

$$\sigma(\omega) = \frac{D}{\pi(\frac{1}{\tau} - i\omega)} \dots \dots \dots (1)$$

where ω is the angular frequency, D is the Drude weight related to the carrier density N and E_F , and τ is the charge scattering time. The fits infer τ and E_F to be 31 ± 2 fs and ~ 0.23 eV for bare graphene, and 29 ± 1 fs and ~ 0.43 eV for monolayer Cu₃BHT-covered graphene. These findings indicate a downshift of E_F in graphene by ~ 0.20 eV upon vdWh formation, corroborating the Raman results.

To further explore the electrical characteristics evolution upon vdWh formation, we calculated their band structures (Fig. 1f) and electrostatic potentials using DFT. The calculated E_F of the vdWh is positioned 0.315 eV below the graphene Dirac cone, signifying a prominent hole accumulation in graphene. Furthermore, we tested three different twist angles, all of which yielded consistent qualitative results, suggesting that the observed effect is independent of interlayer twist and, consequently, the domain position within the polycrystalline material. The charge density difference (CDD) isosurfaces highlight a strong interaction between monolayer Cu₃BHT and graphene (Fig. 1g), leading to electron accumulation in Cu₃BHT and hole accumulation in graphene. These results align with our Raman and TRTS observations and identify that the strong interlayer coupling contributes to significant hole transfer from monolayer Cu₃BHT to graphene upon contact.

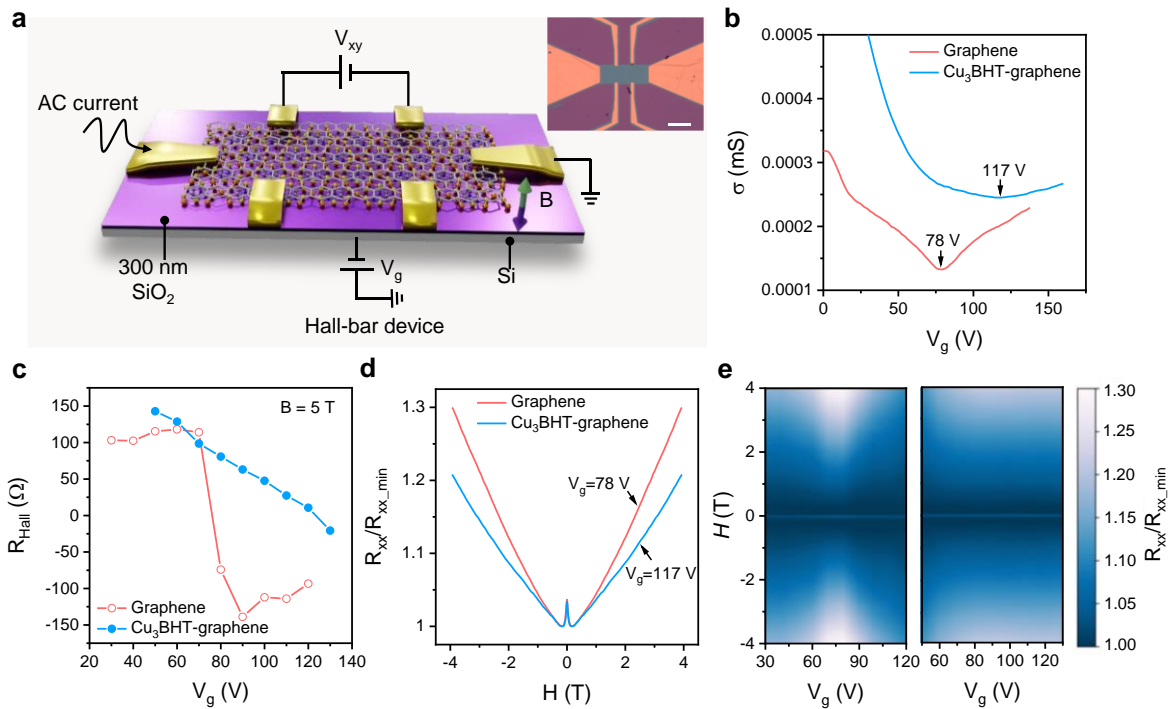


Figure 2| Electrical study of CT in Cu₃BHT-graphene vdWh. **a**, Schematic illustration of the gated-Hall bar device. Inset: Optical image of the gated-Hall bar device. Scale bar, 50 μ m. **b**, Gate-voltage-dependent longitudinal conductance of pristine graphene and Cu₃BHT-graphene vdWh at 2 K, respectively. As the gate voltage increases, the E_F in graphene passes through the Dirac point, leading to a transition in the type of graphene from hole accumulation to electron accumulation. The conductance in graphene initially decreases as the E_F approaches the Dirac point, followed by an increase when the E_F departs from the Dirac point. **c**, Gate-voltage-dependent Hall resistance of pristine graphene and Cu₃BHT-graphene vdWh under 5 T magnetic field, respectively. **d**, Normalized longitudinal resistances R_{xx}/R_{xx_min} of

graphene and Cu₃BHT-graphene vdWh versus field, with applied gate voltage 78 V and 117 V, respectively. A broadened valley manifests that the incorporation of Cu₃BHT indeed impacts the band structure of graphene. e, Mapping of pristine graphene and Cu₃BHT-graphene vdWh's normalized longitudinal resistances R_{xx}/R_{xx_min} , measured with varied magnetic fields and different gate voltages.

We further fabricated gated-Hall bar devices to investigate the electronic properties of Cu₃BHT-graphene vdWh under external electric and magnetic fields (Fig. 2a). As shown in Fig. 2b, the conductance-gate voltage curve of graphene exhibits a distinct minimum at a gate voltage of ~78 V, which corresponds to the Dirac point. In contrast, the Cu₃BHT-graphene vdWh displays a broader valley in the curve, positioned around a gate voltage of ~117 V. This significant shift in the Dirac point suggests the transfer of holes from Cu₃BHT to the graphene layer¹⁹, requiring a higher gate voltage to raise the E_F to the Dirac point. Fig. 2c shows the gate voltage-dependent Hall coefficients, which exhibit reversals of signs at the Dirac points due to the change from hole accumulation to electron accumulation. In pristine graphene, either holes or electrons dominate the Hall signals, leading to a sharp reversal. However, in Cu₃BHT-graphene vdWh, both holes and electrons contribute to the Hall signal, with their respective contributions varying as a function of gate voltage, resulting in a gradual reversal. We further investigate the magnetic field dependence of normalized longitudinal resistance R_{xx}/R_{xx_min} , as presented in Fig. 2d. These curves are interpolated by data points measured at the neighborhoods of their Dirac points. Close to zero field, a small peak is observed, which could be related to weak localization²⁰. The remaining curves exhibit positive magneto-resistance, consistent with the Drude model. The full mapping of gate voltage-dependent magneto-resistance of graphene and Cu₃BHT-graphene vdWh are depicted in Fig. 2e. In graphene, a 130% positive magneto-resistance is observed around the Dirac point, which diminishes significantly as the system moves away from the Dirac point, aligning with previous reports²¹. However, in Cu₃BHT-graphene vdWh, the magneto-resistance remains largely unchanged over a wide range of gate voltages. Collectively, these observations further identify the strong interlayer coupling at the Cu₃BHT-graphene interface.

Discussion

In conclusion, we have demonstrated strong interlayer coupling in a novel Cu₃BHT-graphene vdWh. Vertically stacking monolayer Cu₃BHT and graphene through a wet transfer technique allows facile assembly of Cu₃BHT-graphene vdWhs on the cm² scale with intimate and uniform contacts. As revealed by optical and electrical studies as well as theoretical calculations, the strong interlayer coupling leads to a substantial amount of holes flowing from monolayer Cu₃BHT to graphene upon contact. Our findings lay the foundation for the creation of innovative vdWhs with modulated band alignment and interlayer orbital coupling by integrating monolayer 2DCPs with inorganic 2D materials (e.g., graphene, TMDs, and *h*-BN), and will propel the exploitation of intriguing physical phenomena and specific optoelectronic devices.

Reference

- 1 Hunt, B. et al. Massive Dirac fermions and Hofstadter butterfly in a van der Waals heterostructure. *Science* **340**, 1427-1430 (2013).
- 2 Yankowitz, M., Ma, Q., Jarillo-Herrero, P. & LeRoy, B. J. van der Waals heterostructures combining graphene and hexagonal boron nitride. *Nat. Rev. Phys* **1**,

- 112-125 (2019).
- 3 Liu, Y. et al. Van der Waals heterostructures and devices. *Nat. Rev. Mater.* **1**, 16042 (2016).
 - 4 Jin, C. et al. Ultrafast dynamics in van der Waals heterostructures. *Nat. Nanotechnol.* **13**, 994-1003 (2018).
 - 5 Georgiou, T. et al. Vertical field-effect transistor based on graphene–WS₂ heterostructures for flexible and transparent electronics. *Nat. Nanotechnol.* **8**, 100-103 (2013).
 - 6 Zhou, X. et al. Tunneling diode based on WSe₂/SnS₂ heterostructure incorporating high detectivity and responsivity. *Adv. Mater.* **30**, 1703286 (2018).
 - 7 Withers, F. et al. Light-emitting diodes by band-structure engineering in van der Waals heterostructures. *Nat. Mater.* **14**, 301-306 (2015).
 - 8 Deng, W. et al. Electrically tunable two-dimensional heterojunctions for miniaturized near-infrared spectrometers. *Nat. Commun.* **13**, 4627 (2022).
 - 9 Xia, J. et al. Strong coupling and pressure engineering in WSe₂–MoSe₂ heterobilayers. *Nat. Phys.* **17**, 92-98 (2021).
 - 10 Huang, S. et al. Strain-tunable van der Waals interactions in few-layer black phosphorus. *Nat. Commun.* **10**, 2447 (2019).
 - 11 Van Wijk, M., Schuring, A., Katsnelson, M. & Fasolino, A. Moiré patterns as a probe of interplanar interactions for graphene on h-BN. *Phys. Rev. Lett.* **113**, 135504 (2014).
 - 12 Li, J. et al. General synthesis of two-dimensional van der Waals heterostructure arrays. *Nature* **579**, 368-374 (2020).
 - 13 Sunku, S. S. et al. Photonic crystals for nano-light in moiré graphene superlattices. *Science* **362**, 1153-1156 (2018).
 - 14 McGilly, L. J. et al. Visualization of moiré superlattices. *Nat. Nanotechnol.* **15**, 580-584 (2020).
 - 15 Das, A. et al. Monitoring dopants by Raman scattering in an electrochemically top-gated graphene transistor. *Nat. Nanotechnol.* **3**, 210-215 (2008).
 - 16 Lee, J. E., Ahn, G., Shim, J., Lee, Y. S. & Ryu, S. Optical separation of mechanical strain from charge doping in graphene. *Nat. Commun.* **3**, 1024 (2012).
 - 17 Drude, P. Zur elektronentheorie der metalle; II. Teil. galvanomagnetische und thermomagnetische effecte. *Ann. Phys.* **308**, 369-402 (1900).
 - 18 Drude, P. Zur elektronentheorie der metalle. *Ann. Phys.* **306**, 566-613 (1900).
 - 19 Shin, J. et al. High ambipolar mobility in cubic boron arsenide. *Science* **377**, 437-440 (2022).
 - 20 McCann, E. et al. Weak-localization magnetoresistance and valley symmetry in graphene. *Phys. Rev. Lett.* **97**, 146805 (2006).
 - 21 Cho, S. & Fuhrer, M. S. Charge transport and inhomogeneity near the minimum conductivity point in graphene. *Phys. Rev. B* **77**, 081402 (2008).

Acknowledgments

This work is financially supported by EU Graphene Flagship (GrapheneCore3, No. 881603), ERC starting grant (FC2DMOF, No. 852909), ERC Consolidator Grant (T2DCP), DFG project (2D polyanilines, No. 426572620), H2020-FETOPEN (PROGENY, 899205), CRC 1415 (Chemistry of Synthetic Two-Dimensional Materials, No. 417590517), SPP 2244 (2DMP), GRK2861 (No. 491865171), EMPIR-20FUN03-COMET, as well as the German Science

Council and Center of Advancing Electronics Dresden (cfaed). R.D. thanks Taishan Scholars Program of Shandong Province (tsqn201909047) and National Natural Science Foundation of China (22272092). The authors acknowledge cfaed and Dresden Center for Nanoanalysis (DCN) at TUD and Dr. Petr Formanek, Prof. Andreas Fery, Anna Maria Dominic and Prof. Inez M. Weidinger for the use of TEM facility at IPF, as well as the Raman measurement. We acknowledge SOLEIL for provision of synchrotron radiation facilities and we would like to thank Dr. Arnaud Hemmerle for assistance in using beamline SIRIUS. T.L., M.P. and T.H. thank ZIH Dresden for the use of computational resources.